Additive manufacturing of Ni-based superalloys

Attallah, Moataz; Jennings, Rachel; Wang, Xiqian; Carter, Luke

DOI:
10.1557/mrs.2016.211

Document Version
Peer reviewed version

Citation for published version (Harvard):
Attallah, MM, Jennings, R, Wang, X & Carter, LN 2016, 'Additive manufacturing of Ni-based superalloys: The outstanding issues', MRS bulletin, vol. 41, no. 10, pp. 758-764. https://doi.org/10.1557/mrs.2016.211

Additive Manufacturing of Ni-base Superalloys: The Outstanding Issues

Moataz M. Attallah*, Rachel Jennings, Xiqian Wang, and Luke N. Carter

University of Birmingham, School of Metallurgy and Materials, Edgbaston, B15 2TT, Birmingham, United Kingdom

*Corresponding Author: M.M.Attallah@bham.ac.uk

Abstract

There is an increasing interest in the use of Additive Manufacture (AM) for Ni-base superalloys due to the various applications in the aerospace and power generation sectors. Ni-base superalloys are known to have a complex chemistry, which enables them to achieve their outstanding high temperature mechanical performance, as well as their oxidation resistance, when processed using conventional routes (e.g. casting and forging). Nonetheless, this complex chemistry, with over a dozen alloying elements in most alloys, results in the formation of various phases that could affect the likelihood of their process-ability using AM, resulting in the formation of cracking. Furthermore, due to the directional solidification and rapid cooling associated with AM processes, the alloys experience significant anisotropy due to the epitaxially grown microstructure, as well as the residual stresses that can be sometimes difficult to mitigate using thermal post-processing techniques. This paper aims to highlight the outstanding issues in Ni-base superalloys AM processing, with a special emphasis on the defect formation mechanisms, process optimisation, and the microstructural, mechanical properties, and residual stress development.

Introduction

Ni-base superalloys constitute a class within the broader family of superalloys that contain Nickel as the main alloying element. They possess a combination of outstanding mechanical and physical properties in the temperature range 540˚C to 1000˚C, notably their tensile and creep strength, as well as their resistance to thermal fatigue and oxidation, making them suitable for gas turbine and jet engine components (*1*). The alloying elements are selectively included to improve their performance. For instance, Ti, Al and Nb contribute to the formation of the precipitation strengthening phases (Ni_3Al (γ') and Ni_3Nb (γ'')), which are form as coherent fine precipitates following aging. Other elements (e.g. Ta, Ti, Mo, Hf, W, Cr) contribute to the formation of carbides, which assist in grain size control and resistance to grain boundary sliding at high temperatures. Furthermore, other elements (e.g. Al, Cr, La, Y, Ce) are added to improve their oxidation and corrosion resistance, which is essential to the aforementioned applications (*1*, *2*).

Generally, Inconel 718 (also called Alloy 718) has been the workhorse of the aero-engine sector, due to its combination of good weldability, forgeability, and strength up to 650˚C, at a reasonable cost (*3*). Nonetheless, there has been an increasing interest in the development of Ni-base superalloys that are capable of performing of a higher temperature performance, in order to increase the Turbine Entry Temperature (TET) of gas turbines, which manifests in the improved thermodynamic efficiency (*4*). As a result, newer alloys were developed to achieve this, including CM247LC, RR1000, René41, Hastelloy-X, Waspaloy,

U720, N18, Astroloy, and others (*4*). Despite their outstanding high temperature performance, these alloys are considered to be of limited weldability due to the presence of high γ′-fraction (directly linked to the Ti+Al-content), which increases the susceptibility of the alloys to cracking during post-weld heat treatment (or reheating operations), also known as "strain-age cracking" (*5*). The alloys also become susceptible to ductility-dip cracking, which is associated with the formation of grain boundary carbides (*6*). This relationship between the alloy chemistry and the weld susceptibility is well captured in Figure 1. This does not include other cracking mechanisms (e.g. liquation and solidification cracking), which could occur during welding of most alloys, regardless of the chemistry.

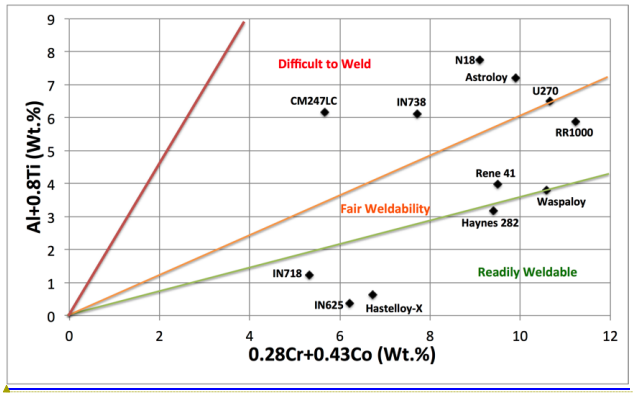

Fig. 1. Weldability assessment diagrams for Nickel-based superalloys using the Cr, Co, Al, and Ti content, after (*7*).

Formatted: Font: (Default) Times New Roman

In simple terms, additive manufacturing (AM) can be described as a multi-layer/repeated welding process. As such, it is susceptible to the formation of weld cracking defects. The processes are associated with rapid cooling rates that were reported to be as high as 10^6 K/s (*8*). This results in the formation of significant residual stresses, as well as an epitaxially-grown microstructure, with both resulting in structural integrity issues and mechanical properties anisotropy. Furthermore, process optimisation for AM techniques, regardless of their type (e.g. selective laser melting/SLM, electron beam selective melting, and direct energy deposition/DED methods) has been performed from an engineering perspective, due to the absence of fundamental understanding of the thermal impact of the process on the microstructure. This review aims to give an overview on the outstanding issues in Ni-superalloys AM, highlighting the key challenges, and the current approaches for their mitigation, as well as some potential that AM may provide in 'tailoring' the material structure.

Residual Stress

Residual stress is defined as stationary stress at equilibrium within a material (*9, 10*). It could arise from the misfit between components, areas within a body or phases (*9, 11*). Therefore, multi-scale residual stresses are determined by their characteristic length: type I macro stresses vary over the dimensions of the component; type II micro stresses span over grain dimensions; type III form at the atomic scale (*9, 11, 12*). Residual stress introduced by AM during layer by layer processing is known to be considerably complex and large (*12, 13*). It is attributed to the large spatiotemporal thermal gradients from localised rapid heating and fast

cooling during processing (*14*). In general, the presence of residual stress within AM parts, especially close to the surface, is undesirable (especially tensile residual stress), as it reduces the effective fatigue and tensile properties ~~when forms near surface~~ and may distort the final geometry (*12, 14, 15*); induces cracks (*12, 13, 16*). When the residual stress overcomes the yield strength of the material, it causes distortion and, as such, a large amount of effort has been invested in the control and reduction of residual stresses (*17-19*).

Experimental measurement of residual stress has been carried out by the hole drilling method (*20, 21*), deflection method (*14, 22*), X-ray diffraction method (*12, 14*), contour method (*15, 23*) and neutron diffraction (*15, 23*). Numerical simulations have also been developed based on finite-elements (FEM) to understand the residual stress development, linking the AM process parameters to melt pool and temperature gradient on the microscopic scale, suggesting approaches for the reduction of the residual stress (*22, 24-26*). On the mesoscopic scale, studies were performed to assess the impact of the thermal field on the residual stress development in individual hatches / layers (*18, 22, 27, 28*). Finally, on the macroscopic scale, investigations were performed to predict the deformation and macrostress (*10, 14, 17, 19, 22*).

In general the study of residual stress has been limited to simple geometries, such as thin walls for both AM manufactured samples and models (*14, 24, 26*), due to the computational cost of performing a fully coupled thermo-mechanical model in large-scale structures. The model results are also in good agreement with the experimental measurements (*19, 29, 30*). Longitudinal residual stress, in tensile nature with parabolic distribution, is found near the top of the samples and tends to increase with the number of deposited layers due to the decreasing thermal gradient (*10, 21, 29, 31-33*). Stresses have also been shown to vary with the height in thin walls, based on the height of the measurement points and the scanning pattern, as longitudinal stresses change from tensile to compressive and may convert to tensile again toward to bottom (*30, 34*). For the normal direction (building direction), residual stress shows compressive in the centre of the wall and gradually reverse to tensile towards to edges due to constraints of base plate from bending deformation, seen in Figure ~~Figure 2~~ (*12, 15, 19, 23, 35*). Further modelling has illustrated that the presence of high tensile stress near the edge is due to the base plate constraining the thin wall from bending rather than the increase of melt pool size (*25*).

Formatted: Font: Not Bold

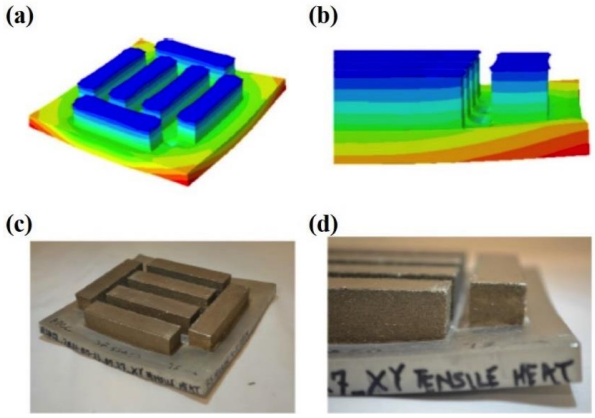

Figure 2. Comparison of warping between simulation results in (a,b) and actual components in (c,d) during EBM of IN718 (*19*).

Theoretical and experimental works have revealed that both the magnitude and trend of residual stress in AM components are governed by material properties (i.e. small coefficient of thermal expansion, large thermal diffusivity, high thermal conductivity) (*14, 27, 35, 36*), phase transformation or precipitation (*12, 23*), geometry of component (*20, 25, 26, 34*), the position of specimens (*20*), processing parameters (*12, 15, 26, 28*), base plate (*10, 19*), and scanning pattern (*10, 18, 22, 23, 27, 34, 37*). It was found that substrate preheating and insulation could help reduce the residual stresses by limiting the thermal gradient between layers and controlling the melt pool, but it may inverse stress from tension to compression (*18, 20, 24, 26, 29, 38, 39*). Shorter scanning vector and larger layer thickness leads less stress due to reduction in the temperature gradient, seen in Figure ~~Figure 3~~ (*10, 13, 17, 22, 23, 30, 37*). Alternating scanning direction also helps lower the stresses (*27, 30*).

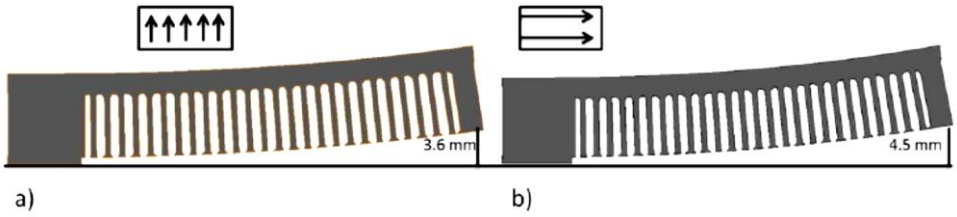

Figure 3. Numerical simulation illustrating deflections between (a) short scanning vector and (b) long scanning vector (*22*).

In summary, it is difficult to create Ni-base superalloy AM structures with reduced residual stresses, which can be effectively mitigated using thermal processing, due to that the insufficient flexibility of the AM platforms and the computational cost of predicting the scanning strategies and process parameters that will result in reduced residual stresses. Future AM platforms should employ physics-inspired scanning strategies that will aim to reduce the thermal stresses through controlling the thermal gradients in complicated 3D

structures. In addition, the hot powder bed systems should be extended to laser-based systems to mitigate the residual stresses *in-situ*, similar to electron beam selective melting systems. Finally, computationally non-intensive codes should be developed to predict the thermal fields and residual stresses, and potentially control the residual stress development on the fly, if these codes can be employed on the AM platforms.

Defect Formation in AM of Ni-base Superalloys: Porosity and Cracking

There are two defects commonly associated with the AM of Ni-base superalloys - porosity and cracking; of these, multiple morphologies can be identified. The prevalence of defect type is influenced by, the AM technique used, the process variables implemented within each technique, and by the composition and morphology of the parent material. Porosity formation in the AM of Ni-base superalloys is predominantly process induced and does not appear to differ significantly between alloy compositions (*40*). It should however be noted that residual porosity in the feedstock material (powder) can significantly differ depending on its production route (e.g. Gas atomisation versus plasma rotating electrode powders), and that, this porosity can be passed to the built part (*41*). Generally, insufficient melting resulting from low energy input or poor powder spreading can lead to the formation of large internal voids (*42*, *43*), following a reducing trend in porosity with the increase in the energy density per area. As the energy input increases, porosity transitions in the following way: lack of fusion (due to incomplete melting or balling), to material consolidation, to keyhole porosity (*40*, *44*). Interestingly, the threshold for consolidation appear less dependent on the Ni-superalloy type as shown in Figure 4, which shows the transition from lack of fusion to consolidation for several Ni-base Superalloys. A similar threshold for consolidation has been seen in DLD processed Hastelloy-X (*45*).

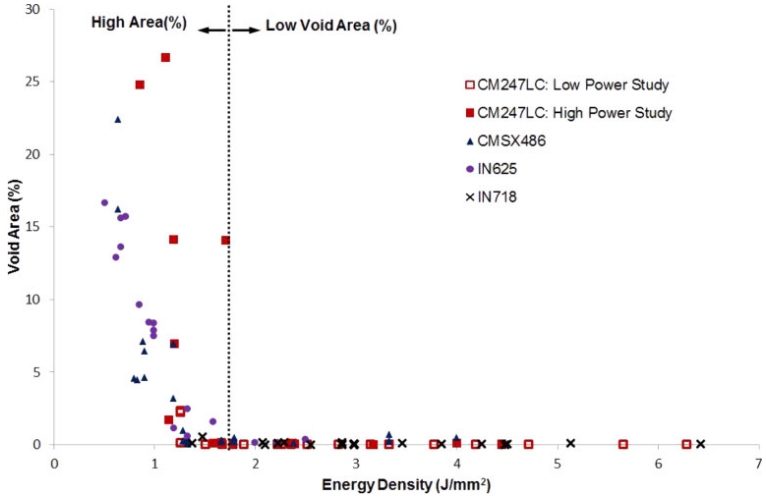

Figure 4.Void area (%) plotted against energy density generated from collated results of five different studies relating to SLM of Ni superalloys (*40*)

Another potential cause for defect formation is balling, which occurs when a track of deposited material has a reduced wettability due to an increase in surface tension; a propensity to minimise the surface energy leads to the formation of balls of material, resulting in a rough surface finish and surface porosity. In SLM and DLD of Ni-base superalloys, balling tends to form when low input energies are used; this can result from an increase in scanning speed (*46*), or a decrease in laser energy (*44*). In addition to this, the formation of oxides owing to insufficient shielding, can also increase surface tension (*47*). However, once the energy density reaches a high level sufficient to trigger the keyhole-welding mode, pores can start to form. Keyhole-induced porosity has been reported to occur in varying geometries according to the spatial level at which it occurs in the keyhole (e.g. the root, middle or top). While there is some debate as to which morphology comes from where, it is generally agreed that the porosity is the result of metal vapour rising out of the keyhole and becoming trapped during keyhole collapse (*48*). Keyhole porosity is quite common in Ni-base superalloys due to the large melting range created by having numerous alloying elements. Keyhole porosity has been reported to increase with increasing energy density (*44, 49*). Peak power has been shown to influence keyhole formation, with a broadening of peak power leading to a reduction in keyholing (*49, 50*).

Whereas for AM-induced cracking, four cracking mechanisms can be identified as resulting from the AM processing of Ni-base superalloys- solidification cracking, liquation cracking, ductility-dip cracking (DDC) and post-weld heat treat (PWHT) cracking (*51*). Rapid cooling during solidification results in the trapping of liquid between already solidified dendrites; when stressed, these weak mushy regions rupture and tear (*51, 52*) creating jagged solidification cracks. Solidification cracking has been seen to occur when high energy densities are implemented during AM (*51, 53, 54*). Conversely, other work has emerged suggesting that high energy densities actually lead to a reduction in cracking (*43, 45*). In addition to this, component size has also been shown to effect the onset of solidification cracking, with larger components producing greater thermal gradients and consequently increased solidification cracking (*53*). Several studies have recently emerged on the effects of Zr-segregation on solidification cracking in IN738LC. It is suggested that Zr-films become trapped between dendrite arms towards the grain boundaries, embrittling the grain boundary region; when stressed, cracks form similar to those of solidification cracking morphology (*49, 55, 56*).

Other studies pointed out to the impact of the scanning strategy on the formation of the solid-state ductility-dip cracking (DDC), pointing out to the role of remelting and rapid solidification in increasing in high-angle grain boundaries and grain boundary phases, which when combined with the high residual stresses lead to the development of DDC (*57*). Welding literature suggests that DDC occurs due to the formation of carbides at grain boundaries (*58*), with some reports also suggesting grain boundary shearing (*59-61*). It should be noted that in the latter case, DDC in Ni-superalloys always forms along regions of high-angle grain boundaries (*62*). Low melting point phases resulting from constitutional undercooling, form in grain boundary regions; when heat is applied, these phases melt and their liquid penetrates the grain boundaries, weakening them, resulting in liquation cracking. Tensile stresses created by contracting material elsewhere pull apart the weakened grain boundaries forming relatively smooth cracks (*51*). Limited studies identified

high energy input during AM as the reason for liquation cracking due to low melting point phases (*63*)~~, attribute cracking to the liquation of low melting point phases~~.

Microstructural Anisotropy

AM techniques generally result in a columnar grain structure, with grains extending over several remelt layers. The rapid solidification, combined with the directionality in the heat losses vertically towards the substrate, results in epitaxial growth in either powder bed or DED methods (*64, 65*), Figure 5. Some variability was observed in SLM fabricated structures, whereby the use of island or chessboard scanning strategies resulted in the formation of nearly-equiaxed grains regions embedded within primarily columnar grains regions (*57*). A similar variation was also observed in DLD methods, and was attributed in that case to the cooling history of the builds, which can be manipulated also using the build strategy (*66*). More importantly, due to the repeated heating nature of the process, the microstructure also shows inhomogeneity on the tens of microns scale, which manifests itself in the 'fish-scale' morphology caused by the repeated heating (Figure 5-a), and the inhomogeneity in grain structure and/or segregation (*67*). The anisotropy in the grain structure is not an issue itself provided that it can be utilized to tailor a specific mechanical performance, similar to the directionality of directionally-cast (DS) structures. Nonetheless, this potential has not been fully exploited by the AM user community. Recent work has shown the potential of AM in controlling both the grain size and crystallographic orientation, by manipulating the process parameters (Figure 5-b). The other challenge associated with the microstructure is the metastable nature of the rapid solidification by-products in the build. Most Ni-base superalloys AM builds either show considerable levels of inter-dendritic segregation, or other undesirable solidification-induced phases (e.g. Laves phase) (*65*). As a result, there is always a need for a post-processing treatment, ranging from hot isostatic pressing (HIPping) to heal the defects caused by the process, in addition to a full solution treatment and aging heat treatment. These post-processing operations obviously add to the cost of AM processes, making them less attractive.

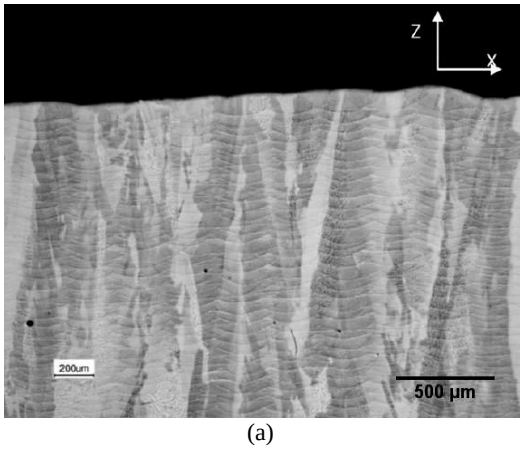

(a)

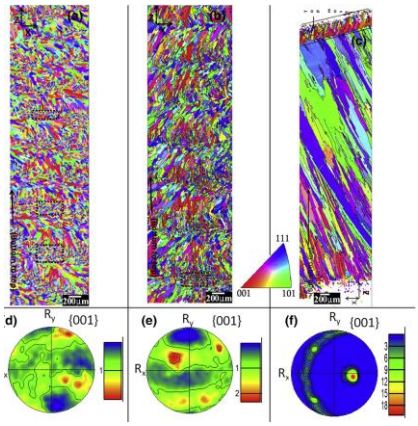

(b)

Figure 5. (a) Coarse columnar grains extending of several layers along the build direction in SLM-processed Nimonic 263, also showing the fish-scale morphology (*68*), and (b) electron-backscattered diffraction (EBSD) maps for DLD-processed IN718, showing the impact of the deposition strategy and laser power on the grain morphology and texture (*65*)

Mechanical Properties

One of the challenges affecting ~~pushing~~ the maturity of AM for Ni-superalloys is the lack of sufficient information in the public domain on their high temperature mechanical performance, notably their creep and high temperature fatigue performance due to the testing cost. Furthermore, the available data were generated through various AM platforms, feedstock material characteristics and chemistry, process parameters, scanning strategies, build/sample geometry, and post-processing treatments, making it highly difficult to have a coherent consensus about the mechanical performance of AM structures.

Figure 6 shows the tensile properties of SLM and DLD-processed IN718, collated from a number of studies. One clear observation is that the as-fabricated properties do not achieve the required performance. Nonetheless, post-processing, whether employing HIPping or not, shows a significant improvement in the tensile properties, especially when a full solution treatment and aging sequence is utilised. Although earlier studies showed strength levels in SLM-processed structures lower than wrought material, a recent study (*69*) showed that strength levels exceeding the wrought condition can be achieved in SLM-processed in IN718 once the post-processing heat treatment is optimised. Nonetheless, heat treatments cannot address the intrinsic anisotropy in the mechanical properties, which usually results in the horizontally built samples slightly over-performing the vertically built samples.

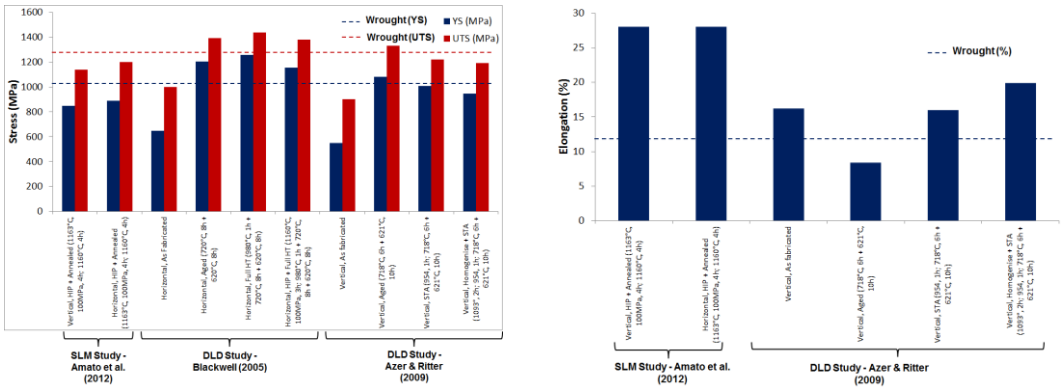

(a) (b)

Figure 6. Collated tensile properties for SLM and DLD-processed IN718 from a number of studies in comparison to wrought IN718 (AMS5662), showing a) ultimate and yield strength and b) tensile elongation % (*41*, *67*, *70*).

Conclusions

Over the last decade, research on AM of Ni-superalloys has addressed a number of material and process challenges. Further work is still required to address the residual stress development, microstructure-properties development and process optimisation, but this depends on the improvement of flexibility in the AM platforms, as well as the development of rapid computational techniques, that can simulate the process to maximise the process and product performance.

References

1. M. J. Donachie, S. J. Donachie., *Superalloys: A Technical Guide*. (ASM International, Ohio, ed. 2nd, 2002).
2. M. Durand-Charre, *The Microstructure of Superalloys*. (Gordon and Breach Science Publishers, Amsterdam, 1997).
3. R. Schafrik, R. Sprague, Superalloy technology - A perspective on critical innovations for turbine engines. *Key Engineering Materials* **380**, 113-134 (2008).
4. R. C. Reed, *The Superalloys: Fundamentals and Applications.*, (Cambridge University Press, 2006).
5. M. B. Henderson, D. Arrell, R. Larsson, M. Heobel, G. Marchant, Nickel based superalloy welding practices for industrial gas turbine applications. *Science and Technology of Welding & Joining* **9**, 13-21 (2004).
6. G. A. Young, T. E. Capobianco, M. A. Penik, B. W. Morris, J. J. McGee, The mechanism of ductility dip cracking in nickel-chromium alloys. *Welding Journal (Miami, Fla)* **87**, 31--43- (2008).
7. E. A. Ott, J. Groh, H. Sizek. (TMS (Minerals, Metals & Materials Society), Warrendale, PA, USA, 2006), pp. 35-45.
8. N. J. Harrison, I. Todd, K. Mumtaz, Reduction of micro-cracking in nickel superalloys processed by Selective Laser Melting: A fundamental alloy design approach. *Acta Materialia* **94**, 59-68 (2015).
9. P. Withers, H. Bhadeshia, Residual stress. Part 1–measurement techniques. *Materials science and Technology* **17**, 355-365 (2001).
10. P. Mercelis, J.-P. Kruth, Residual stresses in selective laser sintering and selective laser melting. *Rapid Prototyping Journal* **12**, 254-265 (2006).
11. P. Withers, H. Bhadeshia, Residual stress. Part 2–Nature and origins. *Materials science and technology* **17**, 366-375 (2001).
12. A. Pinkerton *et al.*, The effect of process parameters on residual stresses within an inconel 718 part produced by the direct laser deposition process. (2005).
13. D. D. Gu, W. Meiners, K. Wissenbach, R. Poprawe, Laser additive manufacturing of metallic components: materials, processes and mechanisms. *International Materials Reviews* **57**, 133-164 (2012).
14. B. Vrancken, R. Wauthlé, J.-P. Kruth, J. Van Humbeeck, in *Proceedings of the solid freeform fabrication symposium*. (2013), pp. 1-15.
15. R. Moat, A. Pinkerton, L. Li, P. Withers, M. Preuss, Residual stresses in laser direct metal deposited Waspaloy. *Materials Science and Engineering: A* **528**, 2288-2298 (2011).
16. M. Zhong, H. Sun, W. Liu, X. Zhu, J. He, Boundary liquation and interface cracking characterization in laser deposition of Inconel 738 on directionally solidified Ni-based superalloy. *Scripta materialia* **53**, 159-164 (2005).
17. L. L. Parimi, M. M. Attallah, J. Gebelin, R. C. Reed, Direct Laser Fabrication of Inconel-718: Effects on Distortion and Microstructure. *Superalloys 2012*, 509-519.
18. N. Klingbeil, J. Beuth, R. Chin, C. Amon, Residual stress-induced warping in direct metal solid freeform fabrication. *International Journal of Mechanical Sciences* **44**, 57-77 (2002).
19. P. Prabhakar, W. Sames, R. Dehoff, S. Babu, Computational modeling of residual stress formation during the electron beam melting process for Inconel 718. *Additive Manufacturing* **7**, 83-91 (2015).
20. C. Casavola, S. Campanelli, C. Pappalettere, Preliminary investigation on distribution of residual stress generated by the selective laser melting process. *The Journal of Strain Analysis for Engineering Design* **44**, 93-104 (2009).
21. M. Griffith *et al.*, Understanding thermal behavior in the LENS process. *Materials & design* **20**, 107-113 (1999).
22. Neugebauer F, Keller N, Hongxiao X, et al. Simulation of selective laser melting process using specific layer based meshing. In: Fraunhofer direct digital manufacturing conference, Berlin, 12–13 March 2014. Stuttgart: Fraunhofer Verlag.~~F. Neugebauer, N. Keller, V. Ploshikhin, F. Feuerhahn, H. Köhler~~.
23. P. Rangaswamy *et al.*, Residual stresses in LENS® components using neutron diffraction and contour method. *Materials Science and Engineering: A* **399**, 72-83 (2005).

24. A. Vasinonta, J. L. Beuth, M. L. Griffith, A process map for consistent build conditions in the solid freeform fabrication of thin-walled structures. *Journal of Manufacturing Science and Engineering* **123**, 615-622 (2001).
25. P. Aggarangsi, J. L. Beuth, M. Griffith, in *Solid Freeform Fabrication Proceedings*. (University of Texas, Austin, TX, 2003), pp. 196-207.
26. J. Beuth, N. Klingbeil, The role of process variables in laser-based direct metal solid freeform fabrication. *JOM* **53**, 36-39 (2001).
27. K. Dai, L. Shaw, Distortion minimization of laser-processed components through control of laser scanning patterns. *Rapid Prototyping Journal* **8**, 270-276 (2002).
28. L. Wang, S. D. Felicelli, P. Pratt, Residual stresses in LENS-deposited AISI 410 stainless steel plates. *Materials Science and Engineering: A* **496**, 234-241 (2008).
29. M. Labudovic, D. Hu, R. Kovacevic, A three dimensional model for direct laser metal powder deposition and rapid prototyping. *Journal of materials science* **38**, 35-49 (2003).
30. M. F. Zaeh, G. Branner, Investigations on residual stresses and deformations in selective laser melting. *Production Engineering* **4**, 35-45 (2010).
31. R. Moat *et al.*, Stress distributions in multilayer laser deposited Waspaloy parts measured using neutron diffraction. (2007).
32. X. Song *et al.*, Residual stresses and microstructure in Powder Bed Direct Laser Deposition (PB DLD) samples. *International Journal of Material Forming* **8**, 245-254 (2015).
33. A. S. C. D'Oliveira, P. S. C. da Silva, R. M. Vilar, Microstructural features of consecutive layers of Stellite 6 deposited by laser cladding. *Surface and Coatings Technology* **153**, 203-209 (2002).
34. S. Zekovic, R. Dwivedi, R. Kovacevic, in *Proceedings SFF Symposium,. Austin, TX*. (2005).
35. N. Shamsaei, A. Yadollahi, L. Bian, S. M. Thompson, An overview of Direct Laser Deposition for additive manufacturing; Part II: Mechanical behavior, process parameter optimization and control. *Additive Manufacturing* **8**, 12-35 (2015).
36. A. Gåård, P. Krakhmalev, J. Bergström, Microstructural characterization and wear behavior of (Fe, Ni)–TiC MMC prepared by DMLS. *Journal of Alloys and Compounds* **421**, 166-171 (2006).
37. A. Nickel, D. Barnett, F. Prinz, Thermal stresses and deposition patterns in layered manufacturing. *Materials science and Engineering: A* **317**, 59-64 (2001).
38. S. Finnie, W. Cheng, I. Finnie, J.-M. Drezet, M. Gremaud, The computation and measurement of residual stresses in laser deposited layers. *Journal of engineering materials and technology* **125**, 302-308 (2003).
39. R. A. Kupkovits, R. W. Neu, Thermomechanical fatigue of a directionally-solidified Ni-base superalloy: Smooth and cylindrically-notched specimens. *International Journal of Fatigue* **32**, 1330-1342 (2010).
40. L. Carter *et al.*, Process Optimisation of Selective Laser Melting using Energy Density Model for Nickel-based Superalloys. (2015).
41. H. Qi, M. Azer, A. Ritter, Studies of standard heat treatment effects on microstructure and mechanical properties of laser net shape manufactured INCONEL 718. *Metallurgical and Materials Transactions A (Physical Metallurgy and Materials Science)* **40**, 2410-2422 (2009).
42. L. N. Carter, K. Essa, M. M. Attallah, Optimisation of selective laser melting for a high temperature Ni-superalloy. *Rapid Prototyping Journal* **21**, 423-432 (2015).
43. M. Ramsperger, R. Singer, C. Körner, Microstructure of the Nickel- Base Superalloy CMSX- 4 Fabricated by Selective Electron Beam Melting. *Metall and Mat Trans A* **47**, 1469-1480 (2016).
44. K. A. Mumtaz, P. Erasenthiran, N. Hopkinson, High density selective laser melting of Waspaloy®. *Journal of Materials Processing Tech.* **195**, 77-87 (2008).
45. F. Wang, X. Wu, D. Clark, On direct laser deposited Hastelloy X: dimension, surface finish, microstructure and mechanical properties. (2011).
46. Q. Jia, D. Gu, Selective laser melting additive manufacturing of Inconel 718 superalloy parts: Densification, microstructure and properties. *Journal of Alloys and Compounds* **585**, 713-721 (2014).
47. S. Das *et al.*, Direct laser fabrication of superalloy cermet abrasive turbine blade tips. *Materials and Design* **21**, 63-73 (2000).

48. P. K. Wei, SC, in *Advances in Multiphase Flow and Heat Transfer,* L. Cheng, Ed. (Bentham Science Publishers, Online, 2009), vol. 1, pp. 213-232.
49. M. Cloots, P. J. Uggowitzer, K. Wegener, Investigations on the microstructure and crack formation of IN738LC samples processed by selective laser melting using Gaussian and doughnut profiles. *Materials and Design* **89**, (2016).
50. H. E. Helmer, C. Körner, R. F. Singer, Additive manufacturing of nickel- based superalloy Inconel 718 by selective electron beam melting: Processing window and microstructure. *Journal of Materials Research* **29**, 1987-1996 (2014).
51. L. Carter, M. Attallah, R. Reed, in *Superalloys 2012*. (Champion, Pennsylvania, 2012).
52. C. Cross, in *Hot Cracking Phenomena in Welds,* T. Böllinghaus, H. Herold, Eds. (Springer, Berlin, 2005), chap. 1, pp. 3-18.
53. D. Dye, O. Hunziker, R. C. Reed, Numerical analysis of the weldability of superalloys. *Acta Materialia* **49**, 683-697 (2001).
54. M. T. Rush, P. A. Colegrove, Z. Zhang, D. Broad, Liquation and post- weld heat treatment cracking in Rene 80 laser repair welds. *Journal of Materials Processing Tech.* **212**, 188-197 (2012).
55. Y.-L. Tsai, S.-F. Wang, H.-Y. Bor, Y.-F. Hsu, Effects of Zr addition on the microstructure and mechanical behavior of a fine-grained nickel-based superalloy at elevated temperatures. *Materials Science & Engineering A* **607**, 294-301 (2014).
56. D. Heydari, A. S. Fard, A. Bakhshi, J. M. Drezet, Hot tearing in polycrystalline Ni-based IN738LC superalloy: Influence of Zr content. *Journal of Materials Processing Tech.* **214**, 681-687 (2013).
57. L. N. Carter, C. Martin, P. J. Withers, M. M. Attallah, The influence of the laser scan strategy on grain structure and cracking behaviour in SLM powder-bed fabricated nickel superalloy. *Journal of Alloys and Compounds* **615**, 338-347 (2014).
58. G. Young, T. Capobianco, M. Penik, B. Morris, J. McGee, The Mechanism of Ductility Dip Cracking in Nickel-Chromium Alloys. *The Welding Journal* **87**, 31-43 (2008).
59. M. L. Collins, JC, An Investigation of Ductility Dip Cracking in Nickel-Based Filler Materials - Part I. *Welding Journal*, 288-295 (2003).
60. M. R. Collins, AJ; Lippold, JC, An Investigation of Ductility Dip Cracking in Nickel-Based Filler Materials - Part II. *Welding Journal*, 348-354 (2003).
61. M. Collins, A. Ramirez, J. Lippold, An Investigation of Ductility-Dip Cracking in Nickel-Based Weld Metals- Part III. *The Welding Journal* **83**, 39-49 (2004).
62. J. Lippold, *Welding Metallurgy and Weldability*. (John Wiley & Sns, Inc. , Hoboken, New Jersey, 2015).
63. G. Bi, A. Gasser, Restoration of Nickel-Base Turbine Blade Knife-Edges with Controlled Laser Aided Additive Manufacturing. *Physics Procedia* **12**, 402-409 (2011).
64. S. Das, Physical Aspects of Process Control in Selective Laser Sintering of Metals. *Advanced Engineering Materials* **5**, 701-711 (2003).
65. L. L. Parimi, G. Ravi, D. Clark, M. M. Attallah, Microstructural and texture development in direct laser fabricated IN718. *Materials Characterization* **89**, 102-111 (2014).
66. F. Liu *et al.*, Microstructure and residual stress of laser rapid formed Inconel 718 nickel-base superalloy. *Optics and Laser Technology* **43**, 208-213 (2011).
67. K. N. Amato *et al.*, Microstructures and mechanical behavior of Inconel 718 fabricated by selective laser melting. *Acta Materialia* **60**, 2229-2239 (2012).
68. T. Vilaro, C. Colin, J. D. Bartout, L. Naze, M. Sennour, Microstructural and mechanical approaches of the selective laser melting process applied to a nickel-base superalloy. *Materials Science and Engineering A* **534**, 446-451 (2012).
69. E. Chlebus, K. Gruber, B. Kuźnicka, J. Kurzac, T. Kurzynowski, Effect of heat treatment on the microstructure and mechanical properties of Inconel 718 processed by selective laser melting. *Materials Science and Engineering: A* **639**, 647-655 (2015).
70. P. L. Blackwell, The mechanical and microstructural characteristics of laser-deposited IN718. *Journal of Materials Processing Technology* **170**, 240-246 (2005).